Electronic Supplementary Information

Surface-Induced Phase Engineering and Defect Passivation of Perovskite Nanograins for Efficient Red Light-Emitting Diodes

Yong-Chun Ye,[a] Yanqing Li,*[b] Yu Tian,[a] Xiao-Yi Cai,[a] Yang Shen,[a] Kong-Chao Shen,[a] Xingyu Gao,[c] Fei Song,[c] Wenjun Wang,[d] and Jian-Xin Tang*[a,e]

[a] *Institute of Functional Nano & Soft Materials (FUNSOM), Jiangsu Key Laboratory for Carbon-Based Functional Materials & Devices, Soochow University, Suzhou 215123, China*

[b] *School of Physics and Electronics Science, Ministry of Education Nanophotonics and Advanced Instrument Engineering Research Center, East China Normal University, Shanghai 200062, China*

[c] *Shanghai Synchrotron Radiation Facility, Zhangjiang Laboratory, Chinese Academy of Sciences, Shanghai, 201204, China*

[d] *School of Physical Science and Information Technology, Shandong Provincial Key Laboratory of Optical Communication Science and Technology, Liaocheng University, Shandong 252059, China*

[e] *Institute of Organic Optoelectronics (IOO) Jiangsu Industrial Technology Research Institute (JITRI), Wujiang, Suzhou 215215, Jiangsu, China*

* Corresponding author. E-mail: jxtang@suda.edu.cn (J.X. Tang); yqli@phy.ecnu.edu.cn (Y.Q. Li)
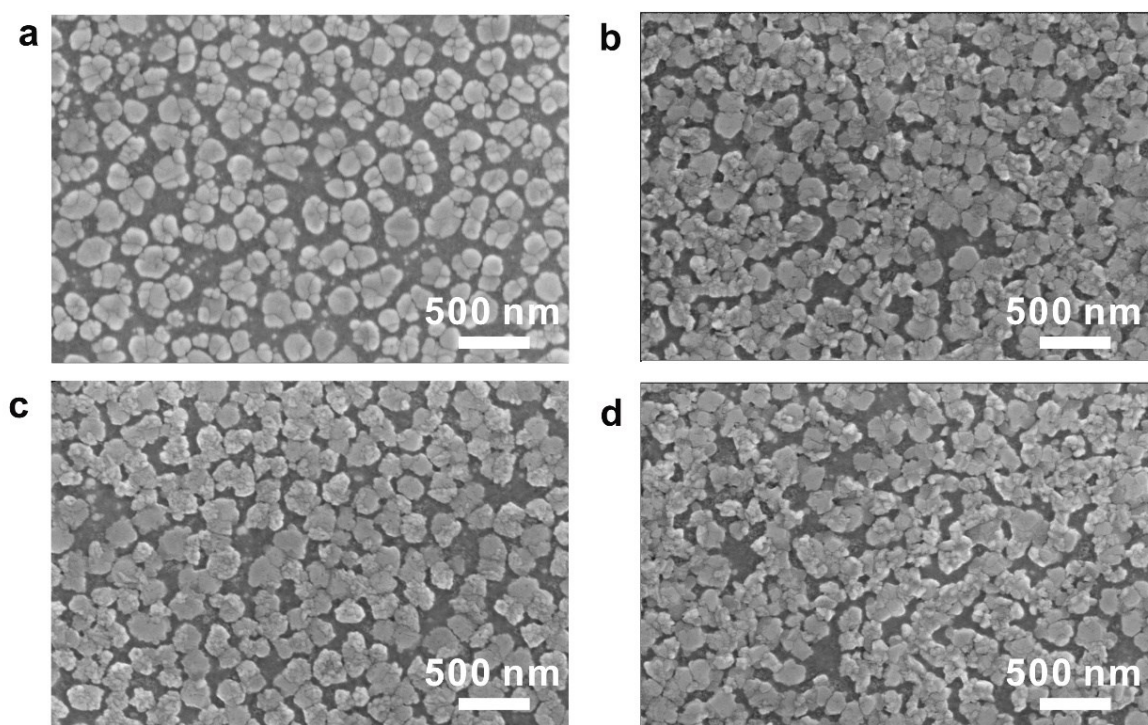
Figure S1. SEM images of perovskite films post-treated with the GAI of the concentrations of (a) 0 mM, (b) 3 mM, (c) 5 mM, and (d) 7 mM, respectively.
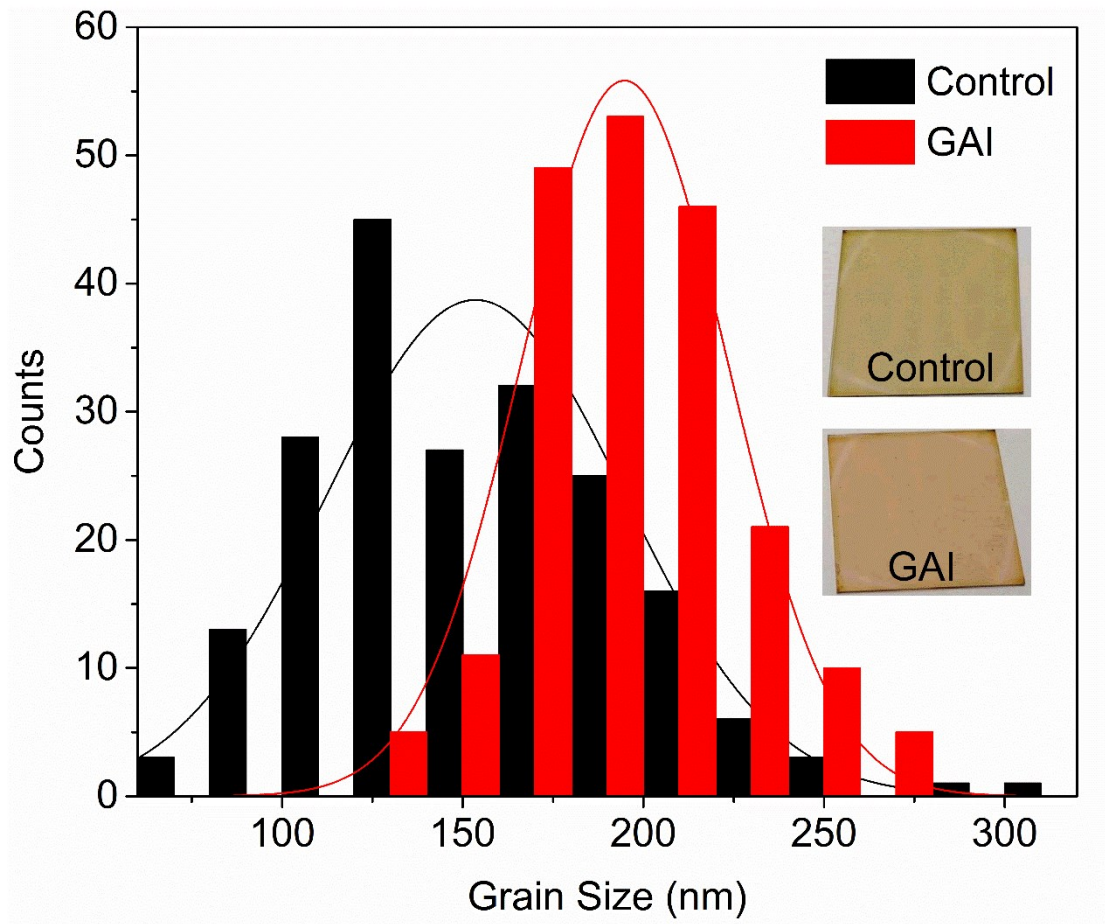
Figure S2. Histograms of the grain size distributions of 200 crystal particles without (control) and with GAI modification as determined from SEM measurements. Insets are the photographs of without and with GAI perovskite films.
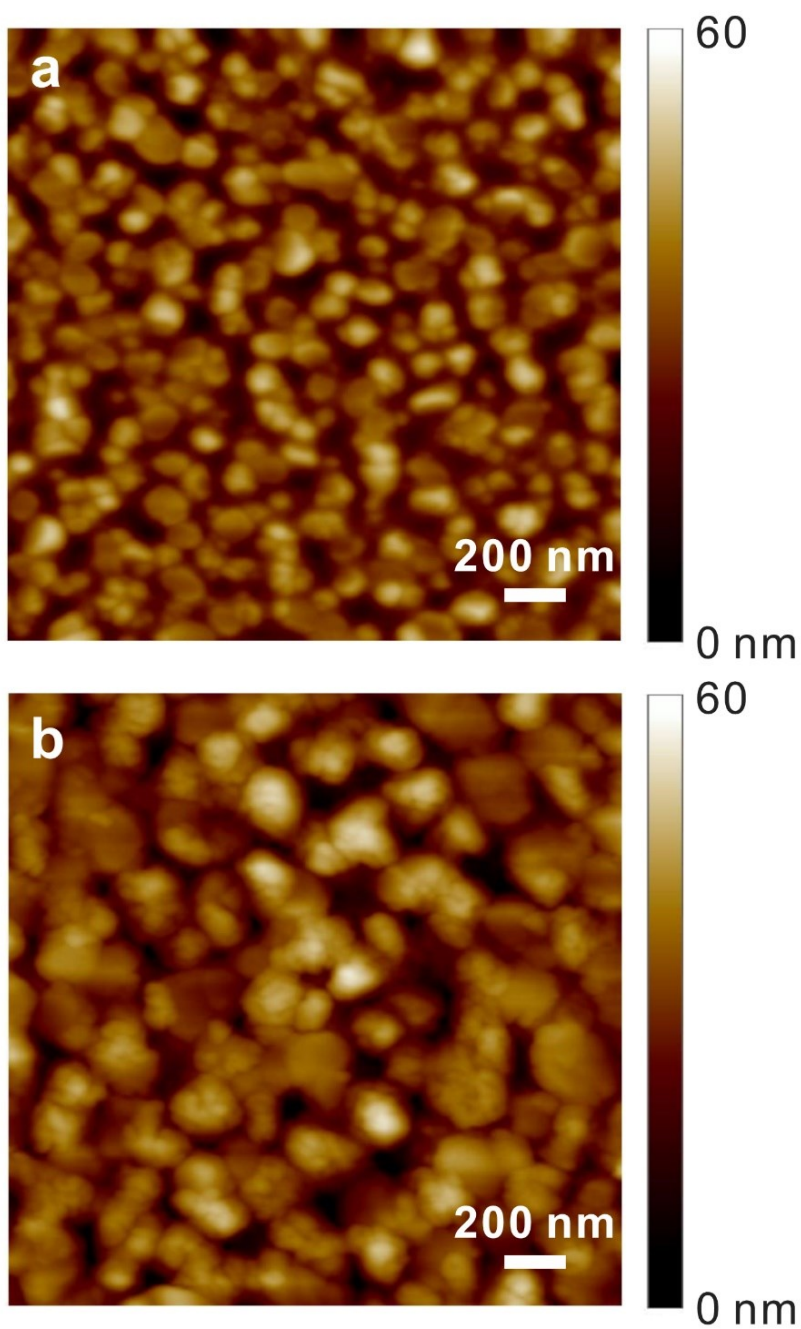
Figure S3. Atomic force microscope (AFM) images of the perovskite films (a) without and (b) with GAI modification.
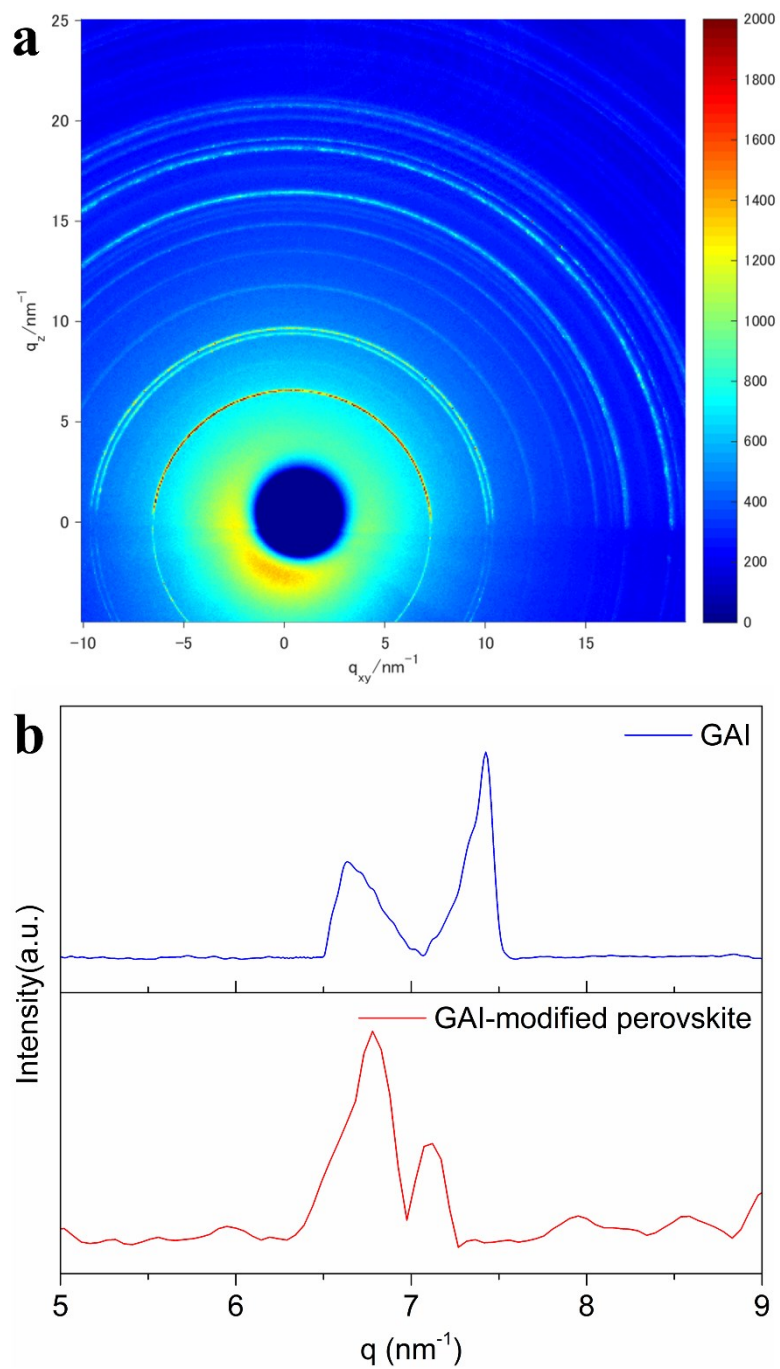
Figure S4. (a) GIXRD pattern of the GAI film. (b) Intensity-dependent q curves of the GAI-modification perovskite film extracted from GIXRD pattern.
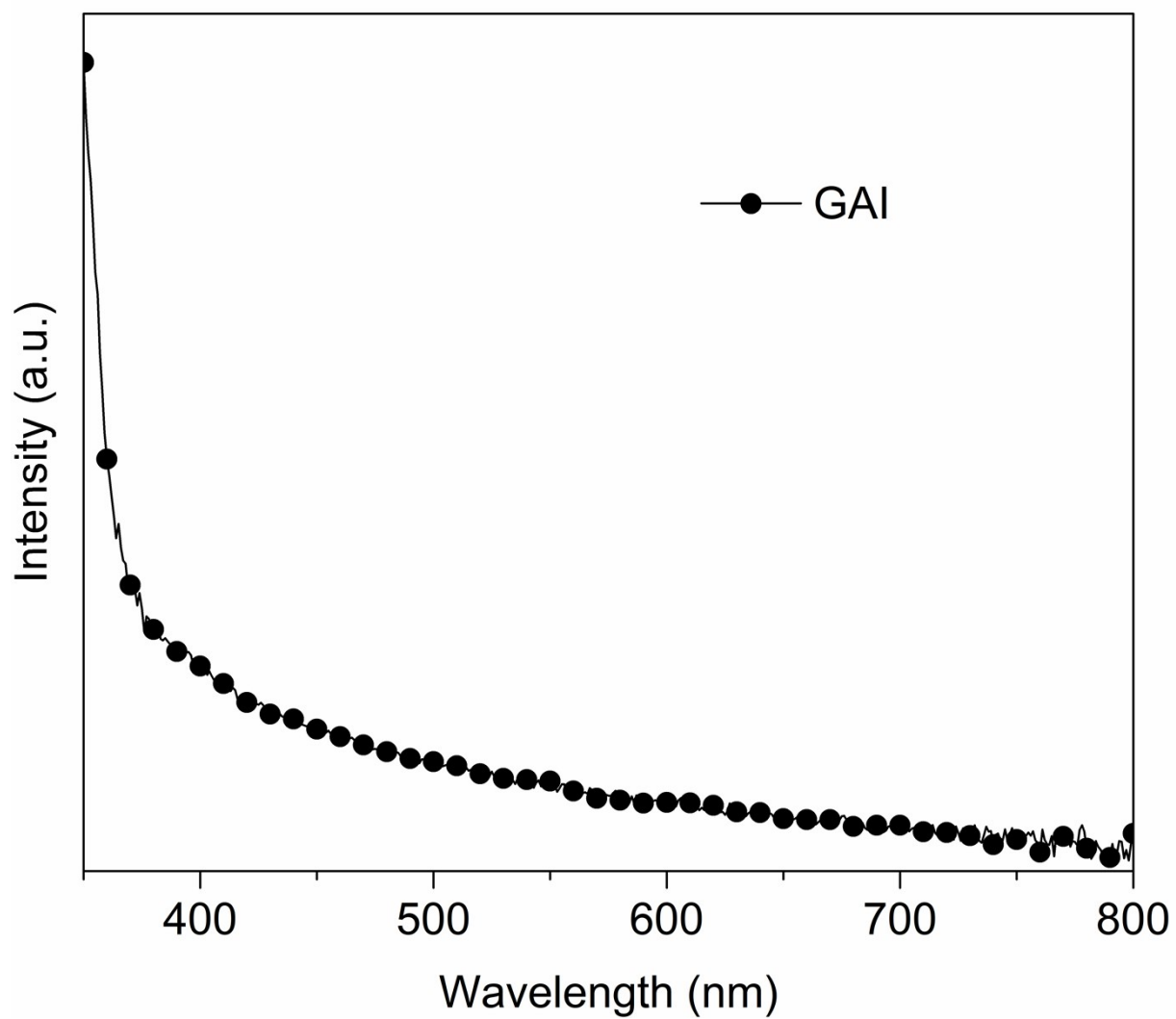
Figure S5. Absorption spectrum of the pure GAI film.
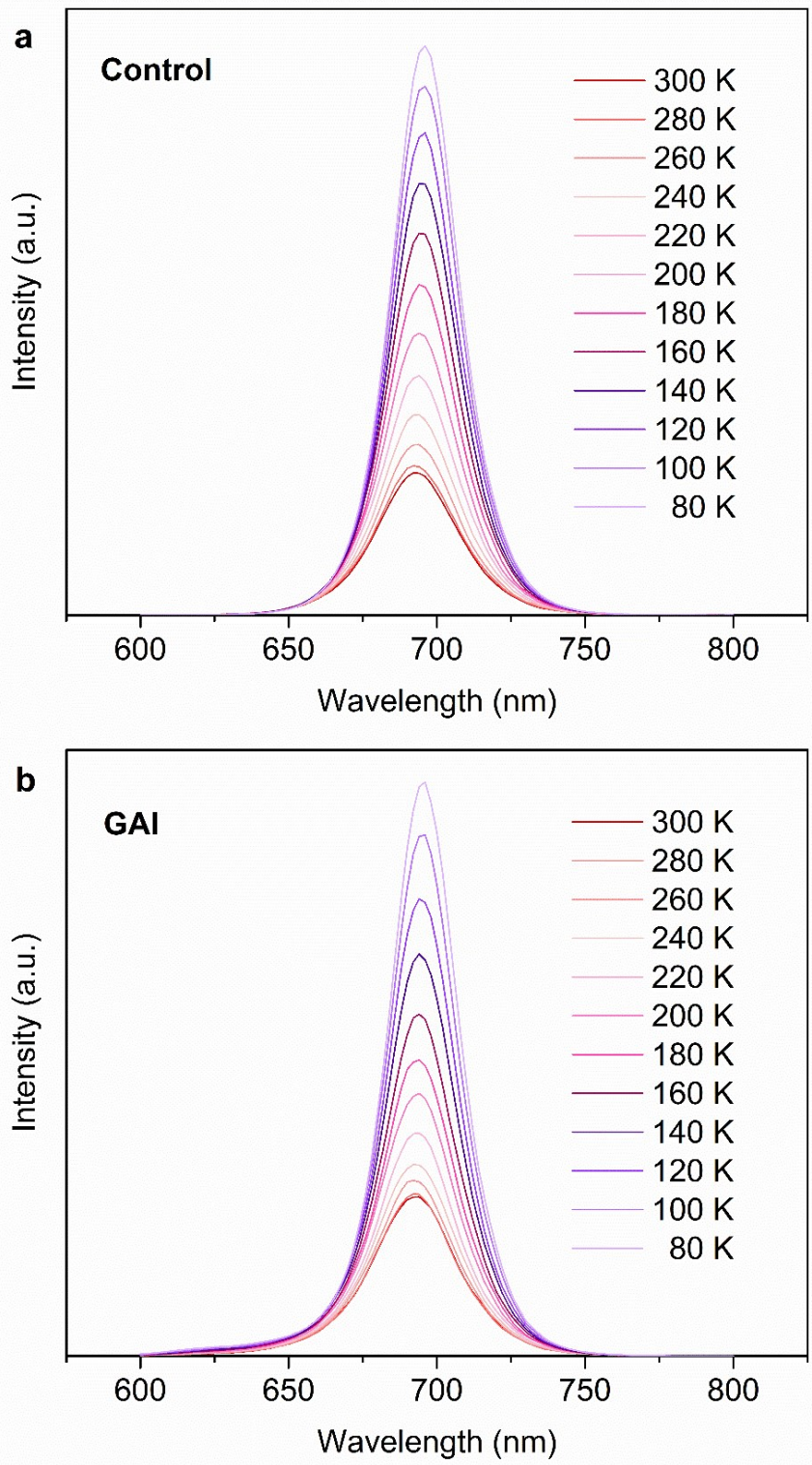
Figure S6. Temperature-dependent PL spectra of the perovskite films (a) without and (b) with GAI modification.
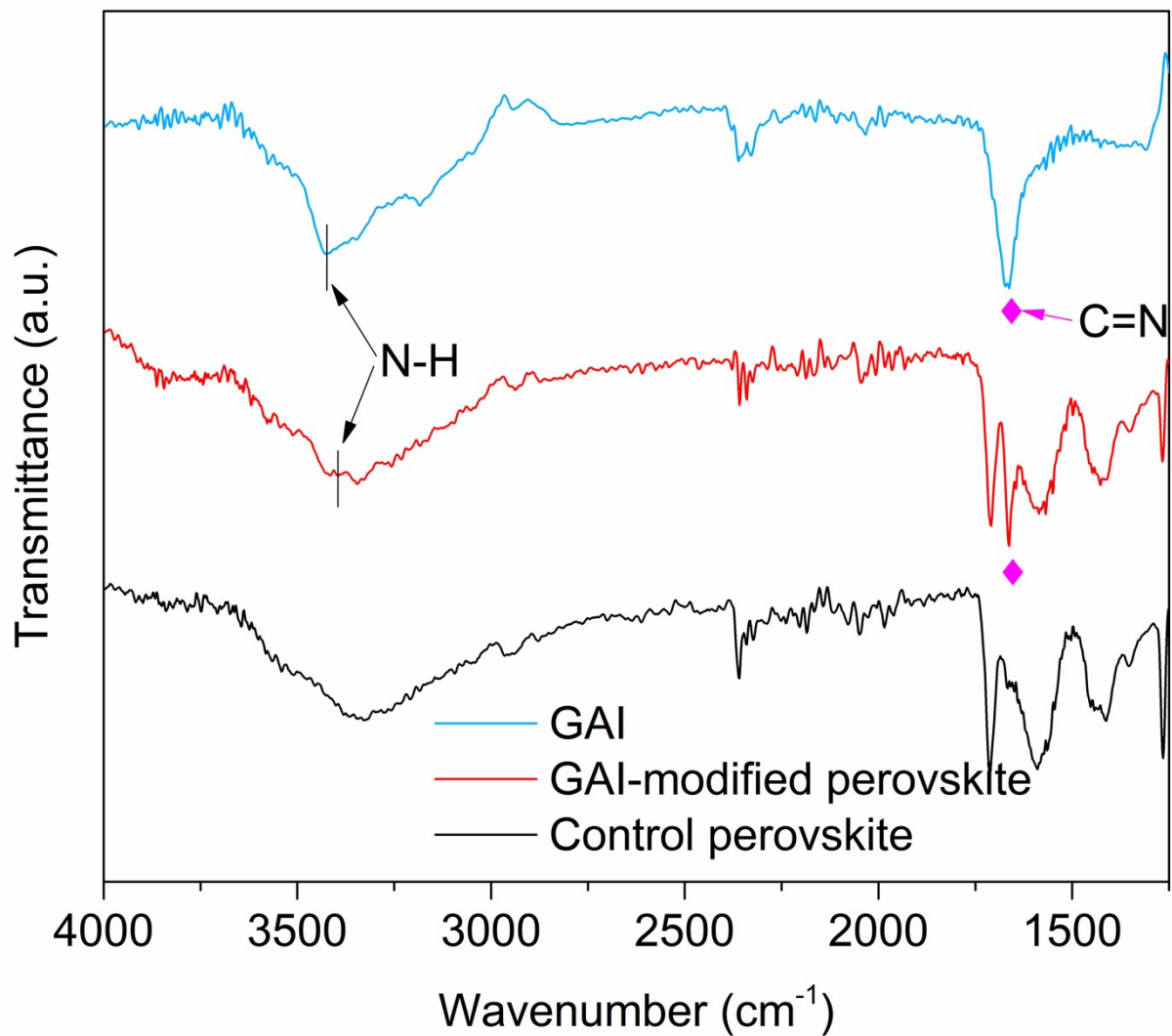
Figure S7. Fourier transform infrared (FTIR) spectroscopy measurement for pure GAI, the control and GAI-modified perovskite films.
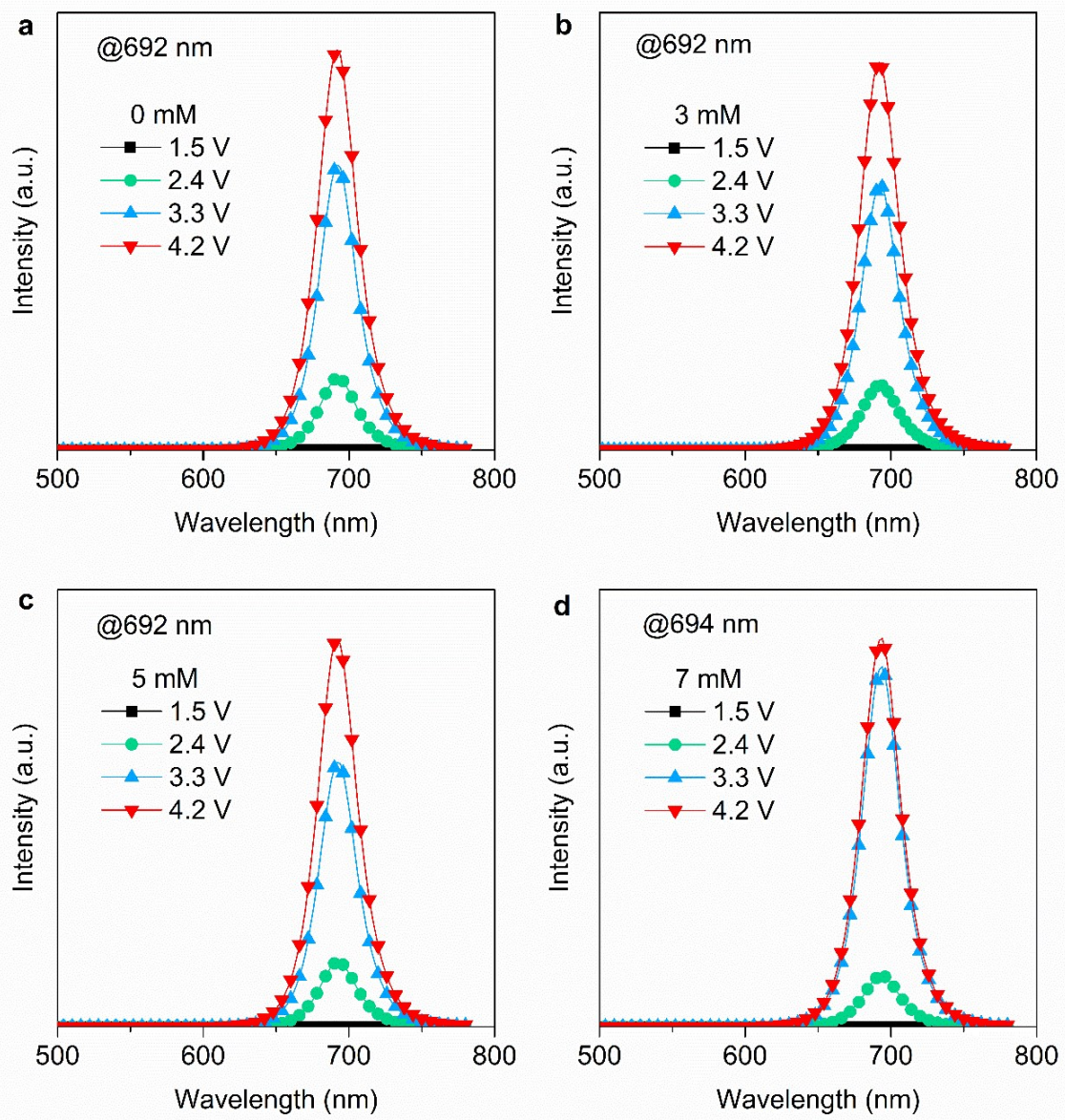
Figure S8. EL spectra at different bias voltages for PeLEDs modified with the GAI of the concentrations of (a) 0 mM, (b) 3 mM, (c) 5 mM, and (d) 7 mM, respectively.
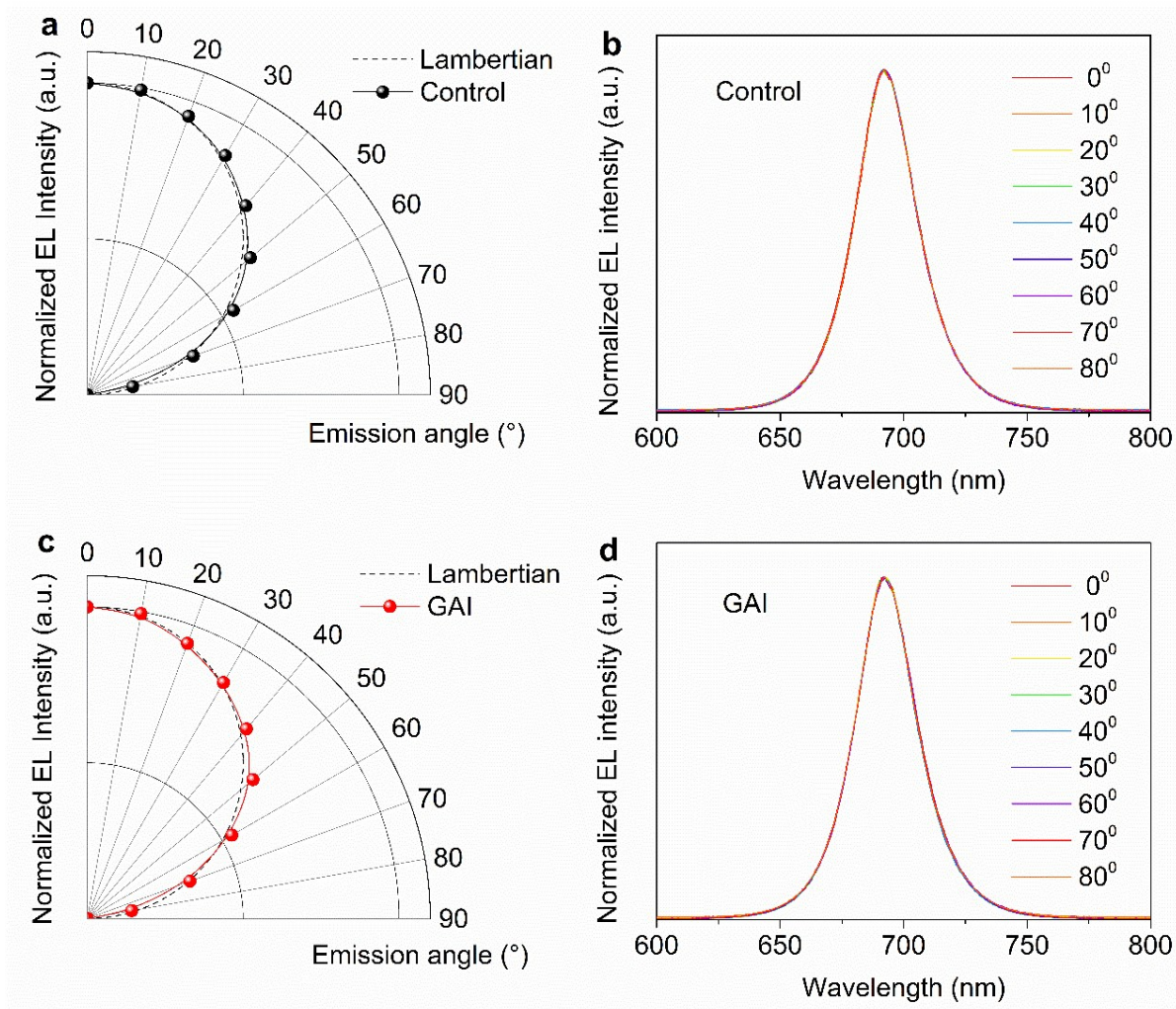
Figure S9. EL characteristics of PeLEDs without and with GAI modification. (a) Angular EL intensity profile and (b) angle-dependent EL spectra of the control device without GAI modification. (c) Angular EL intensity profile and (d) angle-dependent EL spectra of the control device with GAI modification.
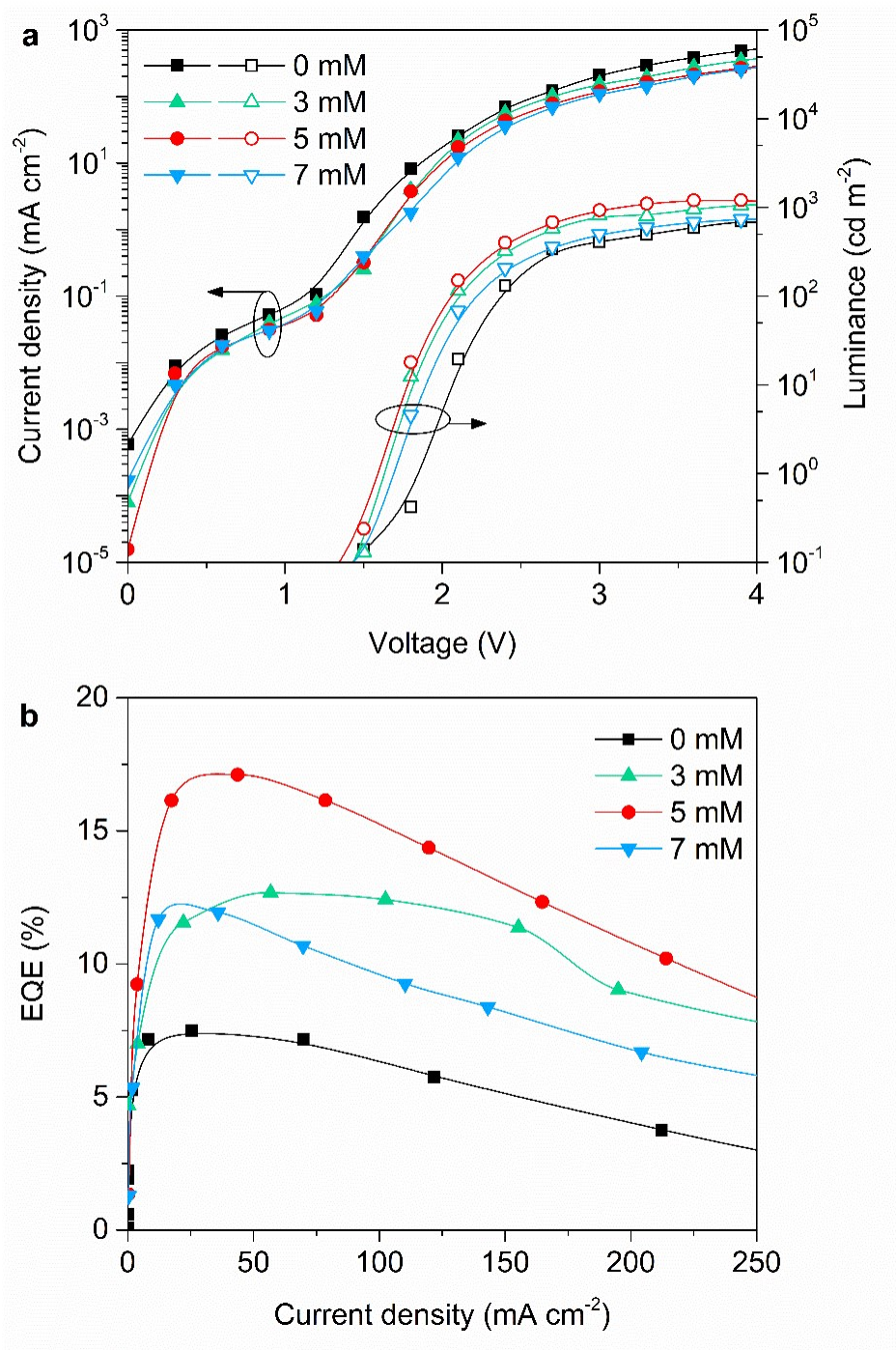
Figure S10. Device performances of PeLEDs modified with various GAI concentrations. (a) I-V-L curves. (b) EQE as a function of current density.
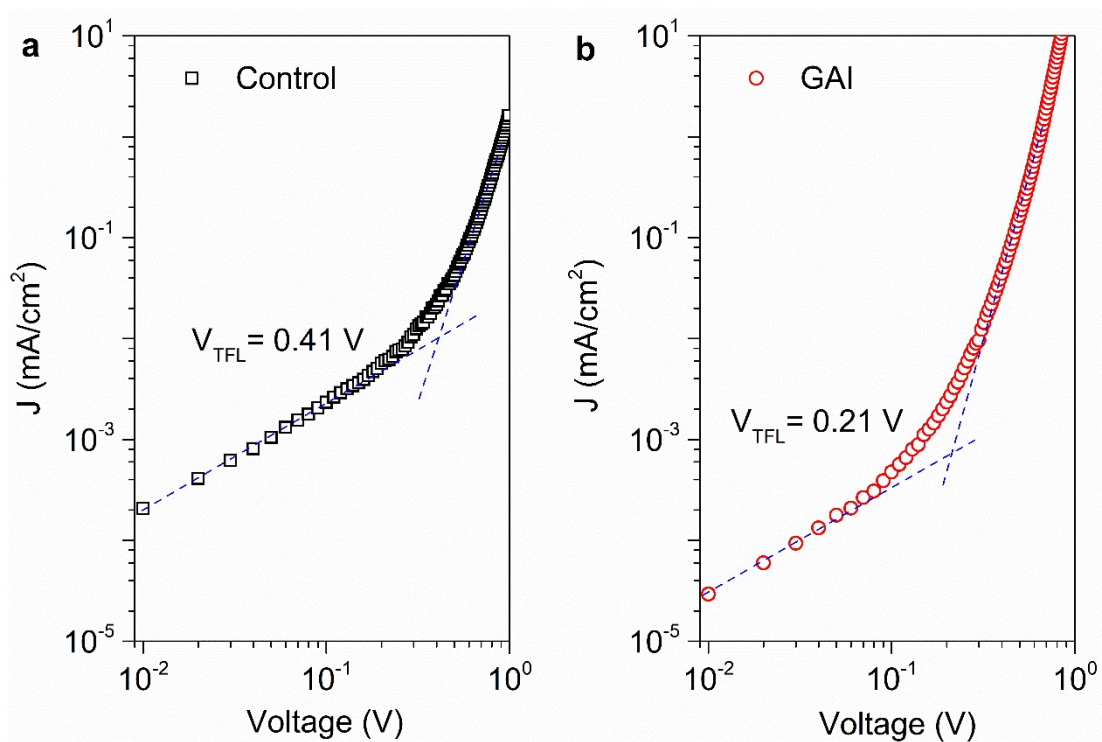
Figure S11. Space-charge-limited current (SCLC) measurements of electron-only devices (a) without and (b) with GAI modification.
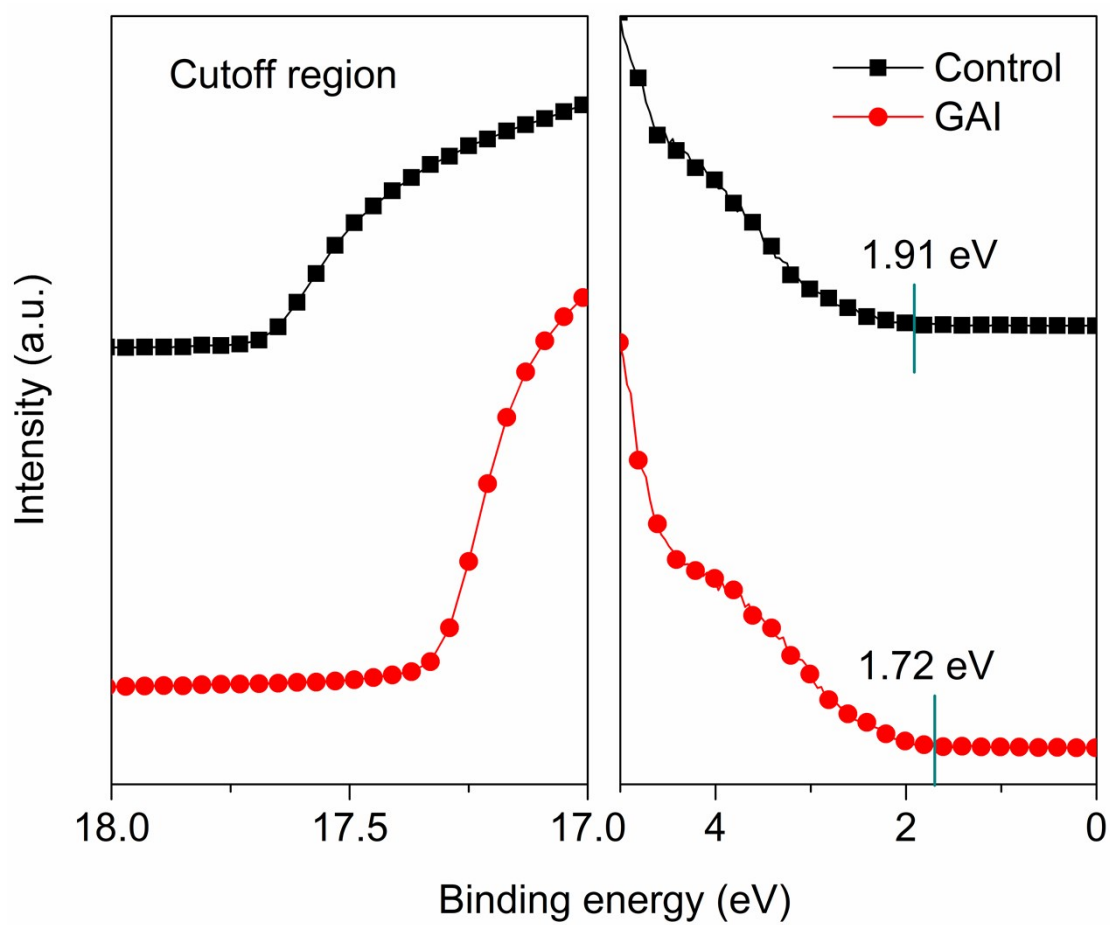
Figure S12. UPS spectra of perovskite films modified without and with GAI (5 mM).

Table S1. Time-resolved PL curve fittings of the perovskite films modified with various GAI concentrations under an excitation pulse at 373 nm.*

Concentration [mM]	PL peak [nm]	FWHM [nm]	τ_1 [ns]	τ_2 [ns]	$\tau_{av.}$ [ns]
0	690	30.8	40	750	289
3	692	32.8	50	1070	427
5	692	33.3	67	1330	686
7	692	34.9	60	1130	563

* The time-resolved PL decay curves measured by time-correlated single-photon counting were fitted by a bi-exponential equation: $Y = A_1\exp(-t/\tau_1) + A_2\exp(-t/\tau_2)$. Here, A_1 and A_2 correspond to the decay amplitudes of fast and slow components, respectively, where $A_1 + A_2 = 1$. The average lifetime τ_{avg} was calculated by $\tau_{avg} = (A_1\tau_1 + A_2\tau_2)/(A_1 + A_2)$.